Ecological Informatics 16 (2013) 17–24

Contents lists available at SciVerse ScienceDirect

Ecological Informatics

journal homepage: www.elsevier.com/locate/ecolinf

Influence of bio-optical parameter variability on the reflectance peak position in the red band of algal bloom waters

Bangyi Tao, Zhihua Mao *, Delu Pan, Yuzhang Shen, Qiankun Zhu, Jianyu Chen

State Key Laboratory of Satellite Ocean Environment Dynamics, Second Institute of Oceanography, State Oceanic Administration, Hangzhou 310012, China

ARTICLE INFO

Article history:
Received 3 December 2012
Received in revised form 8 April 2013
Accepted 13 April 2013
Available online 22 April 2013

Keywords:
Red band
Peak position
Phytoplankton absorption
Chlorophyll fluorescence
Algal bloom
Remote sensing

ABSTRACT

On the basis of field measurements, the quantitatively different relationships of peak position in the red band of the remote sensing reflectance vs. *Chl* concentration are found in the bloom waters of the diatom *Skeletonema costatum* and the dinoflagellate *Prorocentrum donghaiense* in coastal areas of the East China Sea. Model simulations of remote sensing reflectance, R_{rs}, accounting for the influence of variations in the bio-optical parameters such as chlorophyll fluorescence quantum efficiency, Φ, and specific absorption coefficient, a^*_{ph}, are carried out to analyze the characteristics of this spectral peak. The strong effect of fluorescence on the magnitude of R_{rs} results in the inhibition of the shift of the peak to longer wavelengths, increasing Φ enhances this effect. Increasing a^*_{ph}, specifically in the red-wavelength band, causes a sharper shift in the red peak position by decreasing the effect of the fluorescence. The dominant parameter governing the slope of the shift is a^*_{ph}. The analysis indicates that the higher a^*_{ph} *of S. costatum* in the red region is primarily responsible for the much higher slope of the peak shift than for that of *P. donghaiense*. We show that the relationship between the peak position and *Chl* concentration may be useful for discriminating *S. costatum* blooms from those due to *P. donghaiense*, although information about chlorophyll fluorescence quantum efficiency should be included. Finally, we show that using the band ratio R_{rs}(708 nm)/R_{rs}(665 nm) instead of *Chl* in the relationship with peak position can be useful for the practical identification of *S. costatum* blooms from hyperspectral measurements of remote sensing reflectance.

1. Introduction

The remote sensing reflectance (R_{rs}) in the red-wavelength band (650–760 nm), which is less sensitive to the absorption by colored dissolved organic matter (CDOM), has been recognized as a very important wavelength band for monitoring of harmful algal blooms (HABs) in coastal waters. This utility is due to several spectral features unique to phytoplankton that occur in this region (Dall'Olmo and Gitelson, 2005, 2006; Gitelson, 1992; Gons, 1999). Dall'Olmo and Gitelson (2005) and Gitelson et al. (2008) developed red-NIR band ratio models for estimating high chlorophyll concentration in coastal waters. Many papers have shown that these models have a high potential for assisting the development of a simple, universally applicable, NIR-red algorithm (Gurlin et al., 2011; Moses et al., 2012). Cannizzaro et al. (2008) also used the fluorescence/*Chl* ratio to differentiate *Karenia brevis* blooms from other blooms.

Recently, to overcome the difficulty in the remote detection of HABs, some authors used the hyperspectral signatures, specifically the phytoplankton absorption coefficient, $a_{ph}(\lambda)$, to discriminate toxic algal species. For example, based on the fourth derivative of the $a_{ph}(\lambda)$ and the similarity index analysis (Millie et al., 1997), Craig et al. (2006) explored a hyperspectral approach and developed a method to detect *K.brevis* in which the $a_{ph}(\lambda)$ was derived from remote sensing reflectance $R_{rs}(\lambda)$ using a quasi-analytical algorithm (QAA). However, owing to the strong absorption by pure water for wavelengths above 700 nm, $a_{ph}(\lambda)$ cannot be reliably determined in these bands. Consequently, the hyperspectral features in the red band are rarely used in monitoring HABs. In fact, the strong reflectance peak near 700 nm is the most distinguishing feature in the red band. In practice, because of higher radiation energy near this peak compared with peaks in the blue bands, this peak can be more accurately derived by the hyperspectral measurements at the same radiometric noise levels. The peak position can shift from about 680 nm up to 715 nm with increasing chlorophyll concentration (*Chl*), and this red shift has been considered as an important signature for indicating high phytoplankton concentration (Gitelson, 1992). Moreover, during our investigations of algal blooms in the coastal areas of the East China Sea (ECS), the relationship between the position of this peak and the *Chl* concentration are quantitatively different for each algal species. Gitelson et al. (1999) found a similar result in their study. These unique spectral signatures essentially reflect the different optical properties of each algal species, and are potentially useful for taxonomic discrimination of algal species by remote sensing.

Generally, this peak is the result of two intrinsic components: i) an elastic component which corresponds to the combined local minimum

* Corresponding author. Tel.: +86 571 81963115; fax: +86 571 88071539.
E-mail addresses: mao@sio.org.cn, mao99@hzcnc.com (Z. Mao).

1574-9541/$ – see front matter © 2013 Elsevier B.V. All rights reserved.
http://dx.doi.org/10.1016/j.ecoinf.2013.04.005

absorption of phytoplankton and pure water (Vasikov and Kopelevich, 1982), and ii) chlorophyll fluorescence with a maximum near 685 nm (Hoge and Swift, 1987). For low *Chl*, the peak is mostly related to the chlorophyll fluorescence signal, whereas as *Chl* increases this peak begins to be dominated by the elastic component due to the increasing phytoplankton absorption peak around 675 nm. Therefore, the chlorophyll fluorescence quantum efficiency, Φ, and the *Chl* specific absorption coefficient, $a^*_{ph}(\lambda)$ may be the two most important bio-optical parameters. However, the quantum efficiency, Φ, can vary up to a factor of 8 owing to variable phytoplankton taxonomic composition, nutritional status, and temperature (Babin et al., 1996). Further, the chlorophyll specific absorption in the red band, such as $a^*_{ph}(675)$, can also vary up to fourfold as *Chl* concentration varies (Bricaud et al., 1995). Because of the high correlation with the single scattering albedo (ω_0), variable a^*_{ph} can change $R_{rs,}$ originating from the absorption and elastic scattering processes, and also affect the inelastic scattering. Thus, the dependence of features of this spectral peak on the variables Φ and a^*_{ph} can be very complex. To date, precisely how the variations in the bio-optical parameter affect the red peak shift remains unclear. However, uncovering these effects is important for understanding the behavior of the reflectance peak in red band and is necessary to enable the development of practical applications.

The objectives of this study are (1) to access the characteristics of the reflectance peak in the red band of remote sensing reflectance spectra for high chlorophyll, algal bloom waters; (2) to elucidate the underlying physical mechanisms that influence the position of the spectral peak arising from variations in the chlorophyll fluorescence quantum efficiency and the *Chl* specific absorption coefficient; and (3) to analyze the dominant factors resulting in quantitatively different peak position behavior associated with specific harmful algal species. Because *Skeletonema costatum* and *Prorocentrum donghaiense* are the two of the most representative algal species responsible for HABs in the East China Sea, the measured apparent and inherent optical properties of the monospecific species are analyzed to address the aforementioned questions. Such work is essential for understanding spectral behaviors of the red spectral peak for major algal groups and accessing the potential of using red wavelength bands in detecting and identifying HABs.

2. Materials and methods

2.1. Inherent optical property measurements

2.1.1. Absorption measurements

Phytoplankton absorption spectra were determined in two ways. The first method was the quantitative filter technique (QFT) proposed by Tassan and Ferrari (1995). In this method, the spectral absorption coefficients were measured on filter pads (Whatman GF/F) sampled from near-surface bloom waters. This method employs corrections for scattering and path length amplification factors. To avoid errors from scattered light, another method using an integrating sphere with a central cuvette (CIS) system (Nelson and Prézelin, 1993; Röttgers et al., 2007), was also employed for the measurement of suspension samples. This technique improves the absorption measurement by positioning the sample cuvette in the center of an integrating sphere to collect laterally scattered and backscattered light. In this study, the absorption measurements using the second method were made on a Perkin-Elmer Lambda 950 spectrophotometer that consists of a Labsphere 150 mm integrating sphere with a centrally mounted sample holder in which a 1-cm-pathlength cuvette was placed. The total absorption of each algal culture in suspension was always measured against purified water as reference. The absorption of 0.22 μm filtrate of the culture medium was determined in the same way, and subtracted from the total absorption of the algal culture to eliminate molecular scattering and absorption, as well as absorption by any dissolved organic substances produced by the algal cells (Röttgers et al., 2007; Yentsch, 1962). The spectral absorption coefficients for different substances were calculated from the optical density $OD(\lambda)$ as follows:

$$a(\lambda) = 2.303\left(OD_s(\lambda) - OD_f(\lambda)\right)\Big/0.01. \quad (1)$$

The results of the CIS method show good agreement with the QFT results, but show a better performance in the deriving the detailed spectral features.

2.1.2. Total scattering measurements

The scattering coefficient, $b(\lambda)$, can be indirectly obtained from successive measurements of absorption $a(\lambda)$ and attenuation $c(\lambda)$ according to the principle $c(\lambda) = a(\lambda) + b(\lambda)$. Nominally, attenuation coefficients also can be obtained by measuring beam transmittance with a spectrophotometer. To minimize the error of $c(\lambda)$ due to forward scattered light seen by the detector, the attenuation measurements were made on a Perkin-Elmer Lambda 35 spectrophotometer by placing the sample cuvette close to the output window of the sample beam, and the half-angle was reduced to about 0.23° by using an additional custom cuvette with an aperture of 0.8 mm in front of the detector. While $c(\lambda)$ is still underestimated, the error of $c(\lambda)$ was considerably below 5% (Bricaud and Morel, 1986). To avoid errors from multiple scattering within the cuvette, the suspension samples were serially diluted and measurements of absorption and attenuation were made at decreasing concentrations. Only those measurements in which a linear relationship between measured value and the dilution factor was established were utilized. The calculation of $c(\lambda)$ for different substances was the same as that for $a(\lambda)$.

2.1.3. Backscattering measurements

Understanding and quantifying the contribution of algal cells to the backscattering coefficients is essential to bio-optical studies. Bricaud et al. describes an apparatus equipped with an integrating sphere and a tungsten source that is effective for the determination of spectral backscattering by aquatic particulates (Bricaud et al., 1983). The measurements of the light backscattered by particles were carried out by putting a cuvette with a suspension against the exit port of a sphere crossed by a monochromatic beam, and the ratio of the backscattered to incident flux, $R(\lambda)$, was related to the backscattering coefficient, b_b, by the relation:

$$R(\lambda) = 1 - \exp(-kb_b(\lambda)X) \quad (2)$$

where X is the optical path length of the scattering volume, and k depends the geometrical arrangement. In this paper, the incident flux was measured on a standard Spectralon plaque with a nominal reflectance of 99%, placed in the path of the incident beam, and a 10-cm-pathlength sample cuvette was used for the measurements. Similarly, the spectral variation of backscattering by the 0.22 μm filtrate of the culture medium was determined in the same way as the reference to eliminate molecular scattering and specular reflection from the cuvette face.

2.2. Remote sensing reflectance determination

Remote sensing reflectance spectra were derived from above-water measurements of total sea radiance, L_t, sky radiance, $L_{s,}$ and surface downwelling irradiance, E_s, following NASA Ocean Optics Protocols (Mueller et al., 1997). Thus, for each measurement sequence, fifteen successive L_t, L_s and E_s spectra were recorded. L_t and L_s were sampled at a relative azimuth angle of 135° away from the sun and at a zenith viewing angle of 40° according to the configuration proposed by Mobley (1999), E_s spectra were derived by sampling the radiance reflected from a Spectralon plaque with a nominal reflectance of 50%. The measurements were made on the optical instrument of

an Analytical Spectral Devices 512-channel FieldSpec HandHeld spectrometer that provides high spectral resolution radiometric data with a spectral range of 350–1050 nm. In the present study, the in-situ R_{rs} measurements were made on bloom waters that occurred in the Yangtze Estuary, East China Sea from 2009 to 2011. Concurrent *Chl* concentrations were estimated from fluorometer measurements and the dominant algal species of these blooms were identified by microscopic analysis.

2.3. Radiative transfer simulations

The HYDROLIGHT radiance transfer simulations were performed using a two-component model consisting of water and algal particles. Simulations were performed in the VIS and NIR spectral range from 400 nm to 800 nm with IOPs for water taken from the results of Pope and Fry (1997). To explain the effect of the bio-optical parameters of algal culture on the remote-sensing reflectance, specific absorption $a^*_{ph}(\lambda)$ and scattering coefficients $b^*_{ph}(\lambda)$ of each algal culture measured by the above methods were introduced into the model. For simplicity, the phytoplankton absorption coefficient $a_{ph}(\lambda)$ and scattering coefficient $b_{ph}(\lambda)$ for case 2 waters were considered proportional to *Chl* as is often assumed and given by:

$$a_{ph}(\lambda) = Chl \cdot a^*_{ph}(\lambda), \quad b_{ph}(\lambda) = Chl \cdot b^*_{ph}(\lambda). \tag{3}$$

Furthermore, the scattering phase function (SPF) of sea water, $P(\phi)$, is crucial for determining remote-sensing reflectance. Similar to the procedures followed for the total absorption and scattering coefficients, the volume scattering function (VSF), denoted as $\beta(\phi)(=b \cdot P(\phi))$, is composed of contributions from pure water and algal particles, ands can be written as the sum of these two components, expressed in terms of scattering coefficients and scattering phase functions (SPFs), as follows:

$$P(\phi) = \gamma P_w(\phi) + (1-\gamma) P_{ph}(\phi) \tag{4}$$

and

$$\gamma = \frac{b_w}{b_w + b_{ph}} \tag{5}$$

where γ is the probability for a photon to be scattered by water molecules. The pure-water scattering coefficient, b_w, and its SPF, $P_w(\phi)$, have been well studied. SPFs of algal particles, $P_{ph}(\phi)$, are established by employing the phase functions given by the Fournier and Forand (FF) analytic expressions (Fournier and Forand, 1994), which can be derived from the spectrally varying backscattering ratios following the method described by Mobley et al. (2002).

For the calculation of chlorophyll fluorescence effects, the source function of the chlorophyll fluorescence is assumed to have a Gaussian emission around the maximum wavelength, λ_m (i.e. 685 nm), with the width constant and quantum yield (Gordon, 1979) specified in the HYDROLIGHT analysis system. For chlorophyll fluorescence of oceanic phytoplankton, Φ ranges from less than 0.005 to 0.10. In the simulation, the water column was assumed deep enough to avoid any bottom effects, and the IOPs were uniformly distributed throughout the water column. Since light attenuates rapidly in a few subsurface depths in bloom waters, this assumption is considered to be reasonable. Simulations were performed with the sun at zenith, a nominal wind speed of 5 ms^{-1} (to simulate surface roughening), a clear sky, and surface irradiance calculated using the RADTRAN model supplied as part of the HYDROLIGHT code.

3. Results

The R_{rs} data set of algal bloom waters collected in the coastal areas of ESC included two phytoplankton taxonomic groups of *S. costatum* and *P. donghaiense*. R_{rs} spectra varied widely over the visible and NIR spectral regions, and were normalized by the maximum value in the green region and are shown in Fig. 1. They were characterized by minimal values in the blue region (400–500 nm) and two peaks near 560 nm and 700 nm. Importantly, the red shift of peak position was found in both of the R_{rs} spectra sets for the two taxonomic groups. For example, the peak positions in the red band of two spectra for *S. costatum*, highlighted in Fig. 1a, were located at 686 nm at low *Chl* (=4.4 mg/m^3) and shifted to a longer wavelength of 699 nm at high *Chl* (=41.2 mg/m^3). Similarly, the peak positions of two spectra for *P. donghaiense* (Fig. 1b) were found at near 687 nm at low *Chl* (=8.2 mg/m^3) and shifted to around 701 nm at high *Chl* (=112 mg/m^3). The positions of the peak as a function of the *Chl* concentration for the two algal species are shown in Fig. 2. The linear regression shows that the slope of peak position shift with *Chl* concentration in the bloom waters associated with the diatom *S. costatum* (0.400 nm·m^3/mg) is much higher than the one associated with the dinoflagellate *P. donghaiense* (0.158 nm·m^3/mg).

Phytoplankton absorption at 673 nm, $a_{ph}(673)$, ranged from 0.12 m^{-1} to 1.48 m^{-1} with an average value of 0.45 m^{-1}. For the algal bloom waters we investigated, the sum of the absorption coefficients by CDOM and non-algal particles represented less than 2% of the total absorption at 673 nm due their similar spectral shape, which yielded much weaker absorption in the red bands. Therefore the effects of CDOM and non-algal particles were not included in the following analysis and model calculations. Moreover, *Chl* concentration of *S. costatum* samples ranged from near 1.0 to 41.2 mg/m^3 and the values of *P. donghaiense* samples spanned from 4.5 to

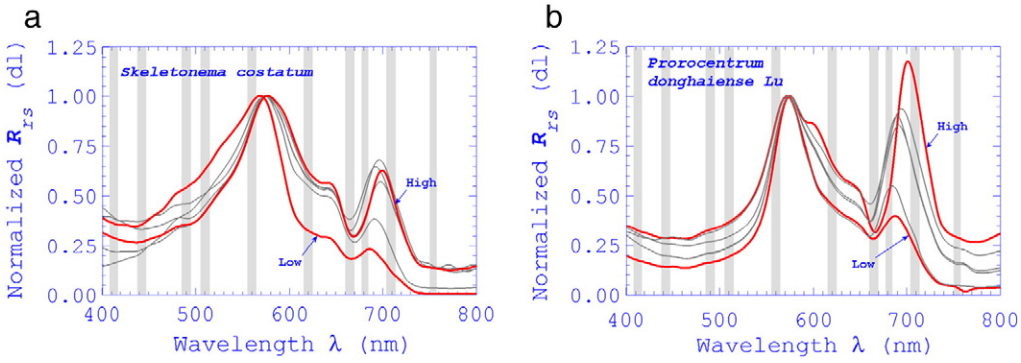

Fig. 1. Observed remote-sensing reflectance spectra of the algal bloom waters normalized by maximum reflectance in the green region. Some examples are highlighted. (a) *S. costatum*: curve "Low," *Chl* = 4.4 mg/m^3; curve "High," *Chl* = 41.2 mg/m^3. (b) *P. donghaiense*: curve "Low," *Chl* = 18.5 mg/m^3; curve "High," *Chl* = 112 mg/m^3. The positions and widths of spectral bands in the MERIS baseline band-set are plotted as gray vertical bars.

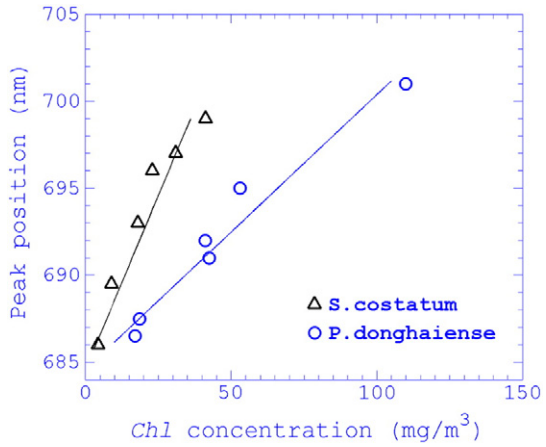

Fig. 2. Relationships of peak position vs. *Chl* concentration associated with *S. costatum* (triangle) and *P. donghaiense* (circle).

112 mg/m^3. As shown in Fig. 3, the chlorophyll specific absorption coefficient at 673 nm, a^*_{ph} (673) of *P. donghaiense* shows a weak relationship with *Chl*, and it ranges between 0.011 and 0.028 m^{2}mg^{-1} with a median value of 0.016 m^{2}mg^{-1}. The values of *S. costatum* vary from 0.021 to 0.035 m^{2}mg^{-1} and yield a lager median value of 0.027 m^{2}mg^{-1}. Although uncertainties introduced by the QFT method and by the *Chl* measurement cannot be ignored, *S. costatum* has a distinctly larger a^*_{ph} in the red spectral range than *P. donghaiense*, which may be related to changes in the packaging effect owing to different phytoplankton groups.

In addition, for the model simulation of R_{rs}, the specific absorption, attenuation, and scattering coefficients ($a^*_{ph}(\lambda)$, $c^*_{ph}(\lambda)$ and $b^*_{ph}(\lambda)$, $bb^*_{ph}(\lambda)$, respectively) were concurrently determined on the suspension samples of the two algal species in the laboratory, based on the methods using the spectrophotometer with an integrating sphere described above. The selected spectra of $a^*_{ph}(\lambda)$ and $b^*_{ph}(\lambda)$ are shown in Fig. 4. The a^*_{ph} of *S. costatum* is higher than that of *P. donghaiense* over almost the whole red-wavelength range, which agrees with the field measurement results using the QFT method. Another distinguishing feature is that b^*_{ph} of *P. donghaiense* increases with increasing λ while that of *S. costatum* decreases with λ. The lower b^*_{ph} *of S. costatum* in the red band will enhanced the absorption of phytoplankton near 673 nm, and may influence the behavior of peak near 700 nm.

To test the radiative transfer model, the HYDROLIGHT computed remote sensing reflectance, which used the measured IOPs as input parameters, is compared to that measured in-situ (Fig. 5). Considering the uncertainties of the measurements involved, agreement is surprisingly good in both magnitude and spectral shape. Because there were no concurrent measurements of fluorescence quantum yield made in-situ, adjustment of Φ gives some flexibility in fitting the reflectance

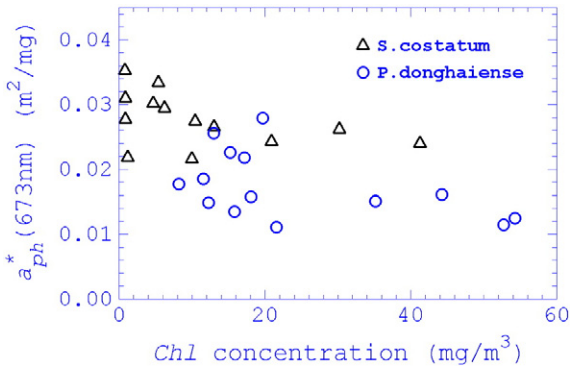

Fig. 3. Chlorophyll specific absorption coefficients at 673 nm of *S. costatum* (triangle) and *P. donghaiense* (circle) as a function of *Chl*.

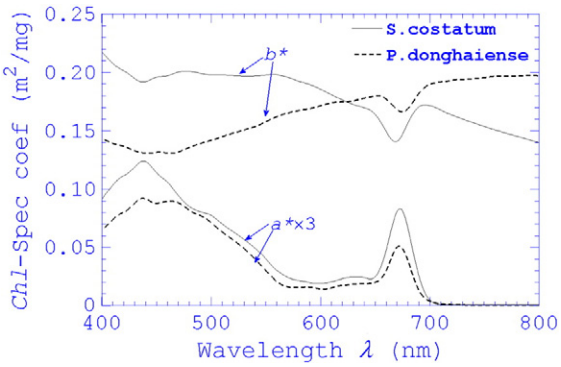

Fig. 4. Spectral *Chl*-specific coefficients (absorption a^* and scattering b^*) between *S. costatum* (solid line) and *P. donghaiense* (dashed line).

level and peak in the red wavelength band. The comparison shows considerable discrepancies in some wavelength bands. One reason for these discrepancies could be errors made during the generation of the calibration coefficients for the radiometer. Because the intensities in the two spectral regions above are generally small, small errors in the calibration procedure would result in relatively large errors during field measurements. The uncertainty in insufficient sky radiance correction for above-water determinations of R_{rs} may be another reason for these discrepancies. Furthermore, the variation in measurements of specific absorption and scattering coefficients used as inputs to HYDROLIGHT may also introduce error to the simulation, but not in the shape of the whole spectrum. Generally, the excellent agreement between the model and measurement indicates that the assumptions in the model are suitable for the R_{rs} simulation of algal bloom waters.

4. Discussion

4.1. Effects of chlorophyll fluorescence

Chlorophyll fluorescence effects, owing to the variability of Φ in algal bloom waters, are first evaluated. For simplicity, in this section, the measured IOPs of *S. costatum* will be used for the detailed investigation in the spectral behavior of the red peak.

Results for the simulated peak position, with and without superimposed fluorescence, are shown in Fig. 6. When the chlorophyll fluorescence is incorporated into the model calculations ($\Phi > 0.0$), the position of the reflectance peaks for lower *Chl* concentrations are almost always located near 685 nm regardless of the quantum efficiency. When the effect of fluorescence was excluded from this

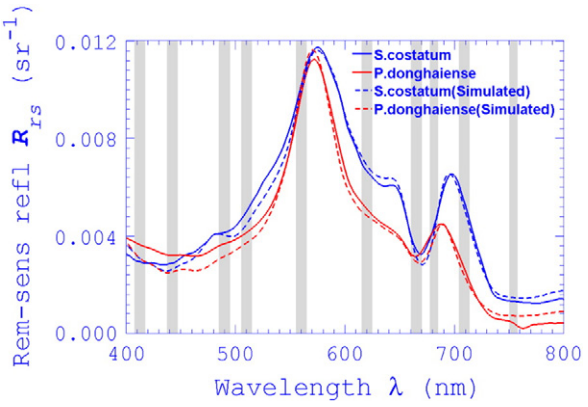

Fig. 5. Comparison of measured remote-sensing reflectance $R_{rs}(\lambda)$ (solid line) and reflectance computed from the HYDROLIGHT (dash line) for *S. costatum* at *Chl* = 41.2 mg/m^3 and *P. donghaiense* at *Chl* = 18.5 mg/m^3. In this model calculation, the fluorescence emission is included.

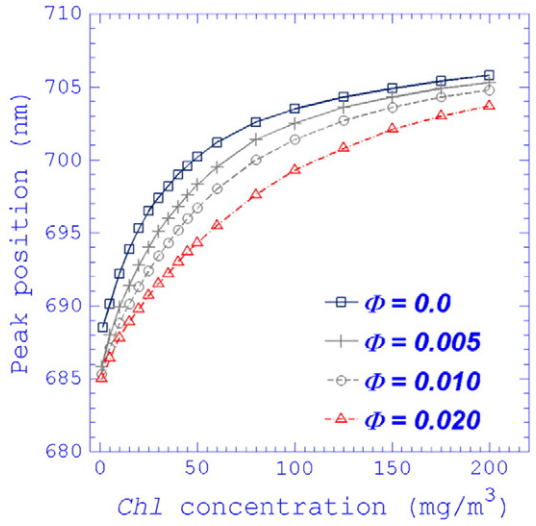

Fig. 6. Model relationships between the spectral peak position and *Chl* concentration for Φ = 0.0, 0.005, 0.01 and 0.02.

calculation, the peak position occurs at a longer wavelength near 690 nm. This fact indicates that the origin of the reflectance peak around 685 nm can be ascribed to fluorescence effects.

All of these calculations show sharp shifts in the peak position with increasing *Chl* concentration, and a saturation near 705 nm which is caused by the very sharp increase in absorption due to pure water beyond 710 nm (Smith and Baker, 1981). The slopes of the relationship between peak position and *Chl* for lower *Chl* (from 10 to 80 mg/m^3) are approximately four times those for *Chl* above 100 mg/m^3. The relationship is specific to each quantum efficiency level. First, the discrepancy of the peak positions between the results including the inelastic fluorescence process and the one obtained in the purely elastic mode is the largest in the range of *Chl* from 10 mg/m^3 to 80 mg/m^3, with a maximum difference of 6 nm for Φ = 0.02 at *Chl* = 60 mg/m^3, and begins to narrow for *Chl* concentrations above 100 mg/m^3. The initial increase can be explained by the strong increase in fluorescence emission with increasing *Chl*. The subsequent decrease arises from the Gaussian-shaped distribution of fluorescence energy that results in a rapid decrease in the fluorescence intensity as the peak shifts away from the optimal emission peak of 685 nm.

For fixed *Chl* levels, while Φ increases from 0.0 to 0.02, the peak position for higher Φ is observed at shorter wavelength, and thus the difference of peak position grows with increasing Φ. In essence, that the peak position is closely related to Φ can be explained by the fact that the chlorophyll fluorescence, with a perpetual emission peak near 685 nm, counterbalances the decrease in reflectance near 675 nm associated with phytoplankton absorption and that higher Φ produces stronger fluorescence emission. These effects result in the maximum reflectance occurring at a wavelength closer to 685 nm and a reduction in the slope of the shift at low *Chl*. In addition, the influence of fluorescence (for Φ higher than 1.0%) on the position cannot be negligible, even for *Chl* greater than 200 mg/m^3. Thus, the shift of the peak position is, to some extent, inhibited by the chlorophyll fluorescence, and the impact of variable Φ is maximal when the Φ is high and the *Chl* is relatively low with peak position closer to wavelength of fluorescence maximum.

4.2. Effects of Chl-specific absorption

Besides the effect of variation in chlorophyll fluorescence quantum efficiency, the absorption due to phytoplankton cells is another important optical parameter that influences the behavior of the position of the peak in the red wavelength band. To investigate the influence owing to the variability of $a^*_{ph}(\lambda)$, we introduce a hypothetical multiplicative factor, *f*, to allow for the artificial modification of $a^*_{ph}(\lambda)$ of *S. costatum* in the spectral region of 645 nm to 700 nm (Fig. 7). This approach is taken in order to isolate the effect of variations in spectral excitation energy on the fluorescence, and thus the R_{rs} in red bands, due to varying specific absorption in the corresponding range of relevant excitation wavelengths. The characteristics of the peak position are essentially systematic variations of R_{rs} in the vicinity of the peak. For a certain *Chl* level, with a given scattering coefficient and fixed SPF, variable *f*, essentially phytoplankton absorption, will change the contributions of both elastic scattering and chlorophyll fluorescence on the R_{rs}, which results in a complex behavior of the position of the peak. To address these, we first define that portion of the R_{rs} contributed by the chlorophyll fluorescence (R_{rsF}) as $R_{rs} - R_{rs\ noF}$ and that the inelastic fluorescence fraction as $100(R_{rs} - R_{rs\ noF})/R_{rs}$ for the remote sensing reflectance. The index *noF* indicates that the inelastic scattering process of chlorophyll fluorescence was excluded from the R_{rs} simulations.

Fig. 8 shows the dependence of R_{rsF} and the fluorescence fraction on *f* and *Chl* concentration at the wavelength of the emission peak of chlorophyll (685 nm). For *f* = 0.6, we find that the R_{rsF} (685 nm) starts at around 0.0018 sr^{-1} at *Chl* = 10 mg/m^3 followed by a strong increase up to 0.004 sr^{-1} at *Chl* = 60 mg/m^3, and nearly levels off at higher *Chl* due to an equilibrium between the elastic and inelastic processes. With increasing *f*, an obvious decreasing R_{rsF} can be seen over the whole range of *Chl*. Inversely, the fluorescence fraction decreases from 52% to 42% as the *Chl* concentration increases from 10 to 100 mg/m^3 when *f* = 0.6, and most interestingly, increasing *f* causes an increase in the fluorescence fraction. These results reveal that an increase of absorption in the red-wavelength band would result in both a decrease in the R_{rsF} and an increase in the fluorescence fraction. The first part of that observation can be explained by the fact that a strong increase in the absorption in the red band increases re-absorption of the fluorescence emission at the same wavelengths, thus reducing the R_{rsF}. A further effect arises from the variation of the elastic scattering. For the given scattering properties, the elastic scattering is reduced by increasing absorption, and probably decreases more sharply than the inelastic scattering of chlorophyll fluorescence.

These variations in R_{rs}, owing to variable a^*_{ph}, naturally have an impact on the peak position. Fig. 9a shows the dependence of peak position on *Chl* concentration for three different *f* factors at two selected values of Φ. When the chlorophyll fluorescence is excluded (Φ = 0.0), for low *Chl* concentrations, the slope of the relationship and the value of the peak position both show noticeable increases with *f*. Similarly, when Φ = 0.02, the position for *f* = 1.4 occurs at a longer wavelength than those for lower *f*. These results reveal that higher specific absorption in the red wavelength band induces a

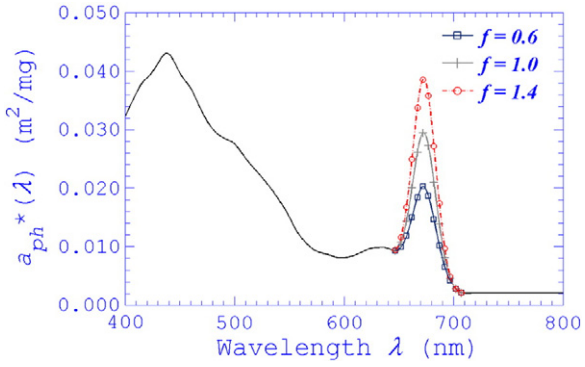

Fig. 7. Chlorophyll-specific absorption spectra (a) in the red band for hypothetical multiplicative factors, *f*, of 0.6, 1.0 (equivalent to observed value) and 1.4 (Φ is set to a constant value of 0.01). The modification of a^*_{ph} only occurs in the specific spectral band from 645 nm to 700 nm.

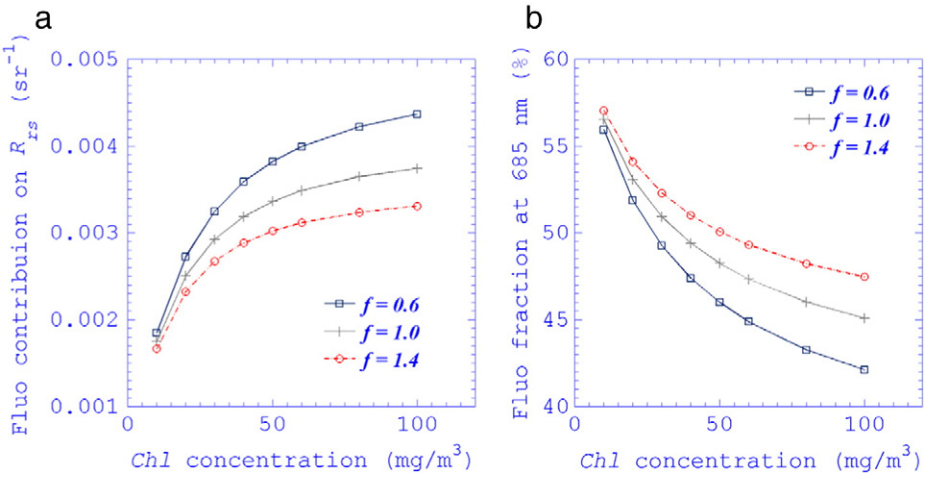

Fig. 8. *Chl* concentration dependence of the fluorescence contribution and fraction for the R_{rs} determined at 685 nm and for factor $f = 0.6$, 1.0 and 1.4 (Φ is set to a constant value of 0.01).

faster shift in the peak position to longer wavelength as the *Chl* concentration increases, and results in the saturation of the peak position near 705 nm at lower *Chl*.

To further investigate the effect of fluorescence on the position of the peak at different values of a^*_{ph}, the difference in the peak position between the two sets of simulated data for each value of *f* are calculated and shown in Fig. 9b. At low *Chl* concentrations, the magnitude of peak position difference increases with the *f* factor. Based on the previous discussion, when the peak is relatively close to fluorescence emission maximum, as *f* increases the fluorescence fraction for the remote sensing reflectance increases and the effect of fluorescence restraining the shift in the peak position is enhanced. However, as the *Chl* increases, the increase in the peak position difference turns into a decrease with increasing *f*. This can be explained by the faster shift of the peak away from the vicinity of fluorescence emission due to higher a^*_{ph}. Therefore, at some point, the absorption is the dominant process governing the shift of the peak position, and an increase in a^*_{ph} would result in a decrease of the effect of chlorophyll fluorescence on the peak position, although the fraction of the fluorescence for R_{rs} is increased at relevant wavelengths.

4.3. Comparison between different harmful algal species

This study has dealt with the analysis of the sensitivity of the R_{rs} peak in the red wavelength band to the chlorophyll fluorescence quantum efficiency and the *Chl* specific absorption coefficient. The last point to consider is the reason for the difference in the slope of peak shift in the bloom waters associated with *S. costatum* and *P. donghaiense*. To address this, the peak positions of *P. donghaiense* simulated in a similar way for varying Φ from 0.0 to 0.02, are shown in Fig. 10 combined with field measurements (in Fig. 2) and model data of *S. costatum* (in Fig. 6). The points associated with *P. donghaiense* are all located in the region bounded by the simulated curves of *P. donghaiense*. However the points associated with *S. costatum* are almost out of that region, and the ones for *Chl* > 20 mg/m^3 are very close to the curve of *S. costatum* with $\Phi = 0.0$. Based on the analysis performed above, the much higher a^*_{ph} and relatively lower b^*_{ph} in the red bands of *S. costatum* can explain much of its sharper peak shift over that seen in *P. donghaiense*.

In fact, the issue of most importance is access to the potential of the inclusion of R_{rs} peak in the red band into models for the identification of algal bloom waters. Due to the quite different spectral behaviors of IOPs in the red wavelength band, it is suggested that the *S. costatum* blooms can be separated from those due to *P. donghaiense* in the peak position to *Chl* phase space. For a given *Chl* concentration, the points associated with *S. costatum* give the highest value of peak position. However, owing to the fact that chlorophyll fluorescence inhibits the red shift and locates the peak position at shorter wavelength, there are overlaps between the curves of *S. costatum* with higher Φ and the ones of *P. donghaiense* with lower Φ values (Fig. 10). Thus, some

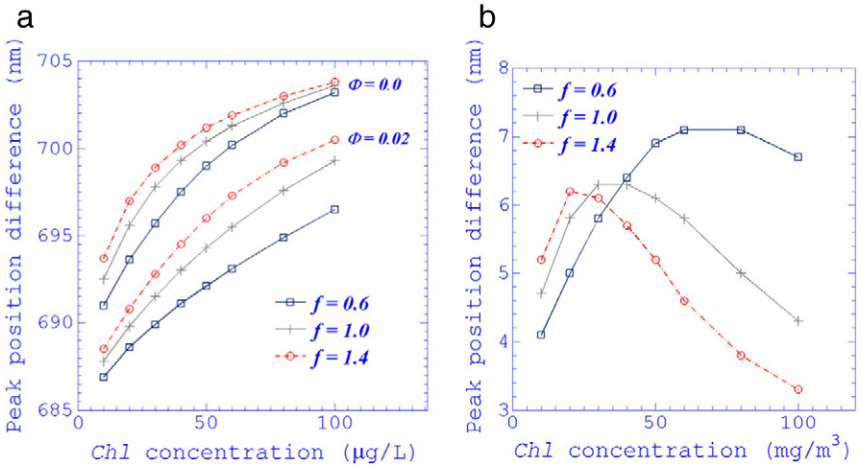

Fig. 9. (a) *Chl* concentration dependence of the peak position for the Φ of 0.0 (three curves on the top) and 0.02 (three ones on the bottom). (b) Difference between the peak positions computed with and without the inclusion of chlorophyll fluorescence, which are calculated from (a). Model calculations are carried out for $f = 0.6$, 1.0 and 1.4.

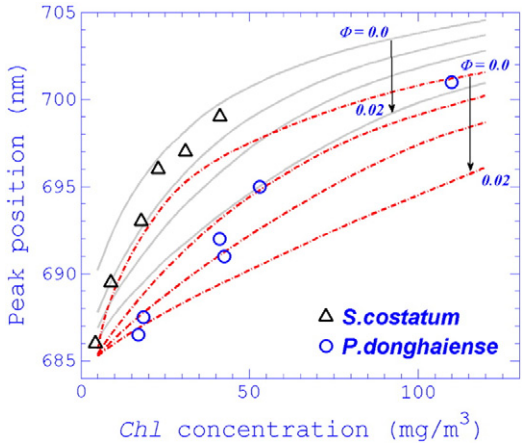

Fig. 10. Variation of relationships of peak position vs. *Chl* concentration associated with *S. costatum* (triangle) and *P. donghaiense* (circle). The solid lines represent the model relationships of *S. costatum* for $\Phi = 0.0$, 0.005, 0.01, and 0.02 from top to bottom. The red dash–dot lines represent the ones of *P. donghaiense* with the same Φs.

points associated *P. donghaiense* at lower Φ could be misidentified as *S. costatum* blooms with higher Φ. This result suggests that the variation of Φ is the most problematic aspect for the discrimination.

Despite the interference owing to the variable chlorophyll fluorescence, this relationship combined with the remote sensing algorithm of *Chl* estimation in algal bloom waters may be applied to remote sensing. The MERIS two-band model (R2), which is developed on the relationship of the band ratio R_{rs}(708 nm)/R_{rs}(665 nm) vs. *Chl*, is a widely used red-NIR band ratio algorithms. This two-band model is considered slightly more accurate than the more complex models in estimation of chlorophyll-a concentrations (Gurlin et al., 2011). Actually, the R2 model is very sensitive to the relationship of *Chl* vs. a^*_{ph} (Gilerson et al., 2010) and hence its calibration coefficients may be specific for the different algal species. Fortunately, there is still a distinguishable discrepancy in the relationships of peak position vs. R_{rs}(708 nm)/R_{rs}(665 nm) for the two specific algal species, even though the peak position and R_{rs}(708 nm)/R_{rs}(665 nm) concurrently change with variations in the a^*_{ph} As seen in Fig. 11, the field measurement data show that the points associated with *S. costatum* can also be discriminated from those due to *P. donghaiense* in the peak position to R_{rs}(708 nm)/R_{rs}(665 nm) phase. These results indicate that the hyperspectral characteristic of peak position shift with *Chl* can be practically applied to the identification of HABs from

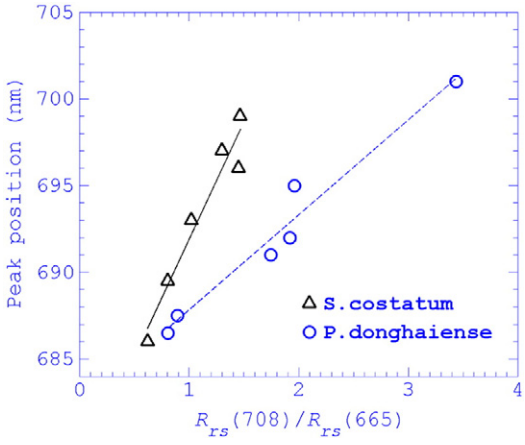

Fig. 11. Comparison of relationships of peak position vs. R_{rs}(708 nm)/R_{rs}(665 nm) associated with *S. costatum* (triangle) and *P. donghaiense* (circle).

measurements of remote sensing reflectance, by using the band ration R_{rs}(708 nm)/R_{rs} (665 nm) instead of *Chl*.

5. Conclusion

In this study, quantitatively different relationships of peak position in red bands vs. *Chl* concentration are found in the bloom waters of *S. costatum* and *P. donghaiense* in coastal areas of ECS. Model calculations accounting for variations in the bio-optical properties, such as the chlorophyll fluorescence quantum efficiency, Φ, and specific absorption coefficient, a^*_{ph}, are provided for the analysis of behaviors of this spectral peak.

Our simulation results showed that the variability of Φ significantly influences the spectral behavior of the peak in the red-wavelength band. The strong effect of fluorescence on the position of the spectral peak cannot be neglected, even at *Chl* greater than 200 mg/m^3 where the purely elastic scattering process dominates the inelastic one. Chlorophyll fluorescence effects inhibit the shifting of the peak position toward longer wavelengths and increasing Φ enhances this effect. Consequently, due to the interference of variations in chlorophyll fluorescence quantum efficiency, the position of the observed spectral peak may be not a stable indicator of the *Chl* concentration.

The analysis also demonstrates the importance of chlorophyll specific absorption coefficients on the characteristics of spectral peak. In opposition to chlorophyll fluorescence, a higher a^*_{ph} in the red band will induce a sharper shift in the red peak position. This is because increasing absorption in the specific red wavelength region of the spectrum results in a strong decrease in the fluorescence induced R_{rs}, despite a simultaneous increase in the inelastic fraction. This results in a decrease in the role of chlorophyll fluorescence in setting the peak position. Therefore, at some point, the dominant parameter causing the red shift of peak position is a^*_{ph}.

Based on the analysis above, the distinctly higher a^*_{ph} in the red region of *S. costatum* is primarily responsible for its sharper shift. The relationship between peak position and *Chl* may be able to be used to discriminate *S. costatum* dominated blooms from *P. donghaiense* dominated ones, although the information about chlorophyll fluorescence quantum efficiency should be included. Finally, we show that using the band ratio R_{rs}(708 nm)/R_{rs} (665 nm) instead of *Chl* can employ the characteristic of peak position shift in the practical identification of *S. costatum* from hyperspectral measurements of remote sensing reflectance.

Acknowledgment

This work was supported by the National Basic Research Program of China ("973" Program, Grant No. 2009CB421202 and 2013CB430302); the National High Technology Research and Development Program of China 863 Program (Grant No. 2007AA092002); the public science and technology research funds projects of the ocean (Grant No. 201005030); the National Natural Science Foundation of China (Grant No. 41206170); the scientific research fund of the Second Institute of Oceanography (Grant No. JG1212 and JG1013); the National Key Technology Research and Development Program of China (No. 2012BAH32B01); and the Postdoctoral scientific research project of Zhejiang Province (Grant No. Bsh1202013).

References

Babin, M., Morel, A., Gentili, B., 1996. Remote sensing of sea surface sun-induced chlorophyll fluorescence: consequences of natural variations in the optical characteristics of phytoplankton and the quantum yield of chlorophyll a fluorescence. International Journal of Remote Sensing 17 (12), 2417–2448.

Bricaud, A., Morel, A., 1986. Light attenuation and scattering by phytoplanktonic cells: a theoretical modeling. Applied Optics 25 (4), 571–580.

Bricaud, A., Morel, A., Prieur, L., 1983. Optical efficiency factors of some phytoplankters. Limnology and Oceanography 28 (5), 816–832.

Bricaud, A., Babin, M., Morel, A., Claustre, H., 1995. Variability in the chlorophyll-specific absorption coefficients of natural phytoplankton: analysis and parameterization. Journal of Geophysical Research 100, 13321–13332.

Cannizzaro, J.P., Carder, K.L., Chen, F.R., Heil, C.A., Vargo, G.A., 2008. A novel technique for detection of the toxic dinoflagellate, *Karenia brevis*, in the Gulf of Mexico from remotely sensed ocean color data. Continental Shelf Research 28 (1), 137–158.

Craig, S.E., Lohrenz, S.E., Lee, Z., Mahoney, K.L., Kirkpatrick, G.J., Schofield, O.M., Steward, R.G., 2006. Use of hyperspectral remote sensing reflectance for detection and assessment of the harmful alga, *Karenia brevis*. Applied Optics 45 (21), 5414–5425.

Dall'Olmo, G., Gitelson, A.A., 2005. Effect of bio-optical parameter variability on the remote estimation of chlorophyll-a concentration in turbid productive waters: experimental results. Applied Optics 44, 412–422.

Dall'Olmo, G., Gitelson, A.A., 2006. Effect of bio-optical parameter variability and uncertainties in reflectance measurements on the remote estimation of chlorophyll-a concentration in turbid productive waters: modeling results. Applied Optics 45, 3577–3592.

Fournier, G.R., Forand, J.L., 1994. Analytic Phase Function for Ocean Water, Ocean Optics XII. SPIE, Bergen, Norway.

Gilerson, A.A., Gitelson, A.A., Zhou, J., Gurlin, D., Moses, W., Ioannou, I., Ahmed, S.A., 2010. Algorithms for remote estimation of chlorophyll-a in coastal and inland waters using red and near infrared bands. Optics Express 18 (23), 24109–24125.

Gitelson, A., 1992. The peak near 700 nm on radiance spectra of algae and water: relationships of its magnitude and position with chlorophyll concentration. International Journal of Remote Sensing 13 (17), 3367–3373.

Gitelson, A.A., Schalles, J.F., Rundquist, D.C., Schiebe, F.R., Yacobi, Y.Z., 1999. Comparative reflectance properties of algal cultures with manipulated densities. Journal of Applied Phycology 11 (4), 345–354.

Gitelson, A.A., Dall'Olmo, G., Moses, W., Rundquist, D.C., Barrow, T., Fisher, T.R., Gurlin, D., Holz, J., 2008. A simple semi-analytical model for remote estimation of chlorophyll-a in turbid waters: validation. Remote Sensing of Environment 112 (9), 3582–3593.

Gons, H.J., 1999. Optical teledetection of chlorophyll a in turbid inland waters. Environmental Science & Technology 33, 1127–1132.

Gordon, H.R., 1979. Diffuse reflectance of the ocean: the theory of its augmentation by chlorophyll a fluorescence at 685 nm. Applied Optics 18 (8), 1161–1166.

Gurlin, D., Gitelson, A.A., Moses, W.J., 2011. Remote estimation of chl-a concentration in turbid productive waters — return to a simple two-band NIR-red model? Remote Sensing of Environment 115 (12), 3479–3490.

Hoge, F.E., Swift, R.N., 1987. Ocean color spectral variability studies using solar-induced chlorophyll fluorescence. Applied Optics 26 (1), 18–21.

Millie, D.F., Schofield, O.M., Kirkpatrick, G.J., Johnsen, G., Tester, P.A., Vinyard, B.T., 1997. Detection of harmful algal blooms using photopigments and absorption signatures: a case study of the Florida red tide dinoflagellate, *Gymnodinium breve*. Limnology and Oceanography 42 (5), 1240–1251.

Mobley, C.D., 1999. Estimation of the remote-sensing reflectance from above-surface measurements. Applied Optics 38 (36), 7442–7455.

Mobley, C.D., Sundman, L.K., Boss, E., 2002. Phase function effects on oceanic light fields. Applied Optics 41 (6), 1035–1050.

Moses, W.J., Gitelson, A.A., Berdnikov, S., Saprygin, V., Povazhnyi, V., 2012. Operational MERIS-based NIR-red algorithms for estimating chlorophyll-a concentrations in coastal waters — the Azov Sea case study. Remote Sensing of Environment 121, 118–124.

Mueller, J.L., Zaneveld, J.R.V., Pegau, S., Valdez, E., Maske, H., Alvarez-Borrego, S., Lara-Lara, R., 1997. Remote Sensing Reflectance: Preliminary Comparisons Between In-water and Above-water Measurements and Estimates Modeled From Measured Inherent Optical Properties, Ocean Optics XIII. SPIE, Halifax, Nova Scotia, Canada.

Nelson, N.B., Prézelin, B.B., 1993. Calibration of an integrating sphere for determining the absorption coefficient of scattering suspensions. Applied Optics 32 (33), 6710–6717.

Pope, R.M., Fry, E.S., 1997. Absorption spectrum (380–700 nm) of pure water. II. Integrating cavity measurements. Applied Optics 36 (33), 8710–8723.

Röttgers, R., Häse, C., Doerffer, R., 2007. Determination of the particulate absorption of microalgae using a point-source integrating-cavity absorption meter: verification with a photometric technique, improvements for pigment bleaching, and correction for chlorophyll fluorescence. Limnology and Oceanography: Methods 5, 1–12 (JAN).

Smith, R.C., Baker, K.S., 1981. Optical properties of the clearest natural waters (200–800 nm). Applied Optics 20 (2), 177–184.

Tassan, S., Ferrari, G.M., 1995. An alternative approach to absorption measurements of aquatic particles retained on filters. Limnology and Oceanography 40 (8), 1358–1368.

Vasikov, A.P., Kopelevich, O.V., 1982. The reasons of maximum at about 700 nm on radiance spectra of the sea. Oceanography (22), 945–950 (% 2012–2010–2007 2022:2031:2000).

Yentsch, C.S., 1962. Measurement of visible light absorption by particulate matter in the ocean. Limnology and Oceanography 7 (2), 207–217.